Influence of the temporal variations of plasma composition on the cyclic formation of dust in hexamethyldisiloxane-argon radiofrequency discharges: Analysis by time-resolved mass spectrometry

Bernard Despax, F. Gaboriau, Hubert Caquineau, Kremena Makasheva

Influence of the temporal variations of plasma composition on the cyclic formation of dust in hexamethyldisiloxane-argon radiofrequency discharges: Analysis by time-resolved mass spectrometry

B. Despax, F. Gaboriau, H. Caquineau, and K. Makasheva

Citation: AIP Advances **6**, 105111 (2016); doi: 10.1063/1.4966254
View online: http://dx.doi.org/10.1063/1.4966254
View Table of Contents: http://scitation.aip.org/content/aip/journal/adva/6/10?ver=pdfcov
Published by the AIP Publishing

Influence of the temporal variations of plasma composition on the cyclic formation of dust in hexamethyldisiloxane-argon radiofrequency discharges: Analysis by time-resolved mass spectrometry

B. Despax, F. Gaboriau, H. Caquineau, and K. Makasheva[a]
LAPLACE (Laboratoire Plasma et Conversion d'Energie), Université de Toulouse, CNRS, UPS, INPT, 118 Route de Narbonne, F-31062 Toulouse cedex 9, France

(Received 11 June 2016; accepted 8 October 2016; published online 21 October 2016)

Cyclic formation of dust nanoparticles in hexamethyldisiloxane (HMDSO, $Si_2O(CH_3)_6$)-argon RF discharge with pulsed injection of HMDSO was studied using time-resolved mass spectrometry (MS) and optical emission spectroscopy (OES). A large amount of C_2H_2, considered as promoter of dust nucleation in hydrocarbon plasmas, was found as a by-product of HMDSO fragmentation. Although no negative ions were detected the presence of C_2H_2 in the HMDSO-Ar discharge supports the hypothesis of a dust growth mechanism based on negative ions being trapped in the plasma. It was found that at the beginning of each cycle of dust formation during α–γ′ transition, the discharge sustaining process is accompanied by a strong consumption of the HMDSO main by-products: HMDSO-15, CH_4 and C_2H_2. At the end of the cycle, corresponding to the progressive disappearance of dust, the discharge switches back to its initial conditions. The beginning of the inverse transition, *i.e.* γ′–α, is most likely correlated to the growing void in the dust cloud and dust disappearance. In presence of dust nanoparticles, Ar^+ and ArH^+ dominate the ion population and consequently the discharge maintenance. When the dust particles gradually disappear, the discharge is rather controlled by $Si_2O(CH_3)_5^+$ ions. Moreover, the increased amount of such heavy ions reveals clearly their important income in the dust repelling process due to the drag force on the large sized dust even at short time scale during the injection time of HMDSO. Atomic-H production increases during the transition from dusty plasma to HMDSO-rich plasma with no dust and its role is associated to a delay in the dust nucleation stage. [http://dx.doi.org/10.1063/1.4966254]

I. INTRODUCTION

The scientific and technological interests in physical phenomena appearing in dusty plasmas have been now maintained for more than two decades, however with different purposes. While in the early 1990's the main aim was to avoid dust formation in reactive plasmas due to its harmful effect in plasma processes in the microelectronic domain,[1,2] the intensive study of dusty plasmas during the last 10 years has drawn benefits from this phenomenon by controlled deposition of nanocomposite thin films through incorporation of the plasma dust into the growing layer.[3] Better understanding, and the following detailed description, of such heterogeneous systems remains an intensive field of research, as they represent interesting building blocks for deposition of multifunctional thin films, and largely add value to development of nanotechnology.

[a]Corresponding author: kremena.makasheva@laplace.univ-tlse.fr

Dust formation in the plasma of hexamethyldisiloxane (HMDSO)-Ar[4] or HMDSO-O_2[5] mixtures was recently reported in the literature. Using HMDSO as a precursor in plasma processing allows depositing polymer-like or silicon oxide thin films (in HMDSO-O_2 mixture) depending on the ratio of the partial pressures of injected gases. Furthermore, HMDSO is non-toxic, non-explosive, and much safer than silane. The experiments described by Despax *et al.*[4] revealed cyclic production/disappearance of dusty plasma induced by the pulsed injection of HMDSO in an argon radiofrequency (RF) axially-asymmetric discharge. The dust presence period (hundredths of seconds) was found to be inversely related to the HMDSO injection time over a given period of the injection pulse (in the seconds range). The larger the quantity of injected HMDSO over a fixed pulse period, the shorter the dust period is. Besides, a complex role of HMDSO and its by-products in the dusty plasma formation and disappearance was suggested.

Periodic appearance of dust particles at very-low frequencies had already been observed in silane[6,7] and Ar-C_2H_2 plasmas[8–12] but not in Ar-CH_4 plasmas.[10,12] For silane plasmas, the new generations of dust were suspected to start growing in the dust-free region, called void, which appears in the central part of the discharge pushing previously formed bigger dust particles toward the plasma edge.[6,7] For C_2H_2 plasmas, the increase of atomic H-amount in the plasma was related to the dust disappearance.[9] This H-increase might be either the cause or the consequence of the dust disappearance. Nevertheless, the authors also showed that adding atomic hydrogen to C_2H_2 plasma can inhibit the formation of dusty plasma.[10] In addition, according to this experiment, the reduction of hydrogen atoms in C_2H_2 plasma leads to the switch from electropositive to electronegative plasma.

Mass spectrometry has been used as a diagnostic technique to detect the potential precursors of dust particles in plasmas of methane, acetylene and ethylene.[8–10,12] The reported results constantly show a large production of acetylenic compounds (C_2H_x). These chemical species appear to be responsible for the production of species involved in dust formation channels whatever the investigated hydrocarbon plasmas. Winter *et al.*[10] have clearly demonstrated that the C_2H_2 concentration is an important factor in the initiation of dust formation for Ar-C_2H_2 and Ar-CH_4 mixtures. However, it seems that the nucleation of dust in Ar-C_2H_2 plasmas also requires the presence of C_2H neutral radicals or C_2H^- ions (above a threshold concentration).[10] This observation agrees with the hypothesis of a dust growth mechanism based on negative ions trapped in the plasma potential. Given that HMDSO has 6 methyl groups, C_2H_2 can be produced in HMDSO-Ar plasma and can play a role in the dust formation process and the observed cyclic behavior. The answer to this question represents one of the objectives of the current study.

A way to initiate dust formation without using hydrocarbon gases is to sustain a RF discharge, usually in Ar, between two graphite electrodes.[13,14] The carbon atoms sputtered from the electrodes produce, after nucleation and probably a very fast coagulation phase, a cloud of carbon nanoparticles that continue to grow by accretion of carbon atoms onto their surfaces. Then, a void appears at the end of the dust cycle when the particles reach a critical size. A periodic phenomenon of dust formation, without a total disappearance of dust, was also observed in this experiment.

Our study concerns an axially-asymmetric discharge in HMDSO-Ar mixture, in which HMDSO electron-dissociation leads to a thin layer deposition on walls as well as on the electrodes. The deposit on the powered electrode can then be sputtered into the discharge. The sputtered atoms and/or organosilicon fragments could play a role on the cyclic dust process. Then the second aspect to consider in our study is oriented to the input of sputtered atoms and/or organosilicon fragments to the cyclic dust process.

A consistent description of the behavior of these complex plasmas requires consideration of different mechanisms, instabilities and forces regarding the dust characteristics, the main plasma parameters, and the interconnection between them. As mentioned above, when particles exceed a critical size, their number density progressively drops as they escape from the plasma. Due to the collective behavior of the plasma these processes involve changes in the mechanisms responsible for the discharge sustaining. To describe the evolution of dusty plasmas Fridman *et al.*[15] proposed that during the coagulation phase, when the particle size becomes larger than a specific value (6 nm in SiH_4-Ar plasmas), the discharge undergoes the so-called α–γ' transition. This transition in the discharge sustaining mechanism differs from the well-known α–γ transition in capacitively-coupled RF plasmas in which the main plasma parameters (electron density and electron temperature) are set

out by the ionization in the plasma bulk that counterbalances the loss of charged species on the walls after their diffusion and electron attachment in the case of electronegative gas. This determines the α–regime of discharge sustaining. In pure argon plasma the α–γ transition appears for high power density when the main source of electrons in the discharge becomes the secondary electron emission from the electrodes, which prevails the ionization in the plasma bulk. In dusty plasmas, when the attachment of negatively charged species on the dust becomes possible, the fast coagulation phase turns out to be an additional channel of loss of charged species. Moreover, the attachment time for particles greater than 2 nm in size is shorter than their residence time in the discharge. Thus, the attachment probability increases as it also allows the particles to be trapped in the plasma. The α–γ′ transition mechanism occurs when the electron loss on the particles exceeds the electron loss towards the reactor wall. To account for this additional mechanism of loss of charged species the electron temperature increases to favor the volume ionization. The dust size-dependent character of the α–γ′ transition imposes the abrupt time-dependent increase of the electron temperature in the beginning of the coagulation phase. Such electron temperature increase reflects a rise of the ionization in the plasma bulk due to the high electric field needed to balance the local loss of charged species.[16,17] The α–γ′ transition mechanism was experimentally detected in dusty plasmas. An important increase of the electron temperature and a strong decrease of the electron density were measured when dust particles became detectable in the plasma which confirms the transition character of the discharge sustaining.[18,19] At the final stage of the dusty plasma period, when dust particles gradually disappear from the discharge a large asymmetric void was observed in our discharge.[4,19] According to Samsonov and Goree,[14] the instabilities of dusty plasma and the subsequent creation of a void in the dust cloud are due to the following mechanisms: (*i*) the electrons are depleted in the dust cloud; (*ii*) the onset of the variation of plasma parameters is triggered by a specific particle size; (*iii*) the ionization in the plasma bulk is enhanced, visually represented by an enhanced plasma glow; (*iv*) the ion drag force is partly responsible for the void formation. However, in contrary to the observations reported in Ref. 14, the increase of dust number density and the enhanced plasma glow in our discharge conditions are in phase with one another. After the dust disappearance the plasma parameters (electron density and electron temperature) return to their initial values. The α–γ′ transition and the creation of a void in the dust cloud appear periodically with successive generations of dust in HMDSO-Ar plasmas with HMDSO pulsed injection. Our understanding is that those two processes control the periodicity in the formation/disappearance of successive generations of dust particles.

In this work the temporal evolution of HMDSO and its by-products is followed by mass spectrometry and optical emission spectroscopy during the cyclic production of dusty plasma. A special focus is made on the production and the time evolution of the main neutral species and positive ions in the plasma at different time scales. This approach allows identifying the leading interactions between the electrons and the different dominant species. Moreover, it indicates the respective contribution of various ions in the discharge sustaining and their impact on the formation/disappearance of dusty plasma. Instabilities of the dust cloud induced by the pulsed injection of the reactive HMDSO precursor are observed and commented.

II. EXPERIMENTAL PART

The 13.56 MHz plasma reactor used in our experiment has been described in details elsewhere.[20] A schematic top view of the experimental arrangement is given in Fig. 1. The gap between the RF-driven top electrode (10 cm in diameter) and the larger bottom electrode (12 cm in diameter) is 3.5 cm. The top electrode is covered by a silver target. The bottom electrode and the reactor walls were grounded. This reactor design produces axially-asymmetric plasma inducing a self-bias voltage on the powered electrode. The self-bias voltage scales up with the injected power in the discharge. The experiments in this work were carried out with a - 600 V self-bias voltage, corresponding to a RF power P = 30 W. Argon was used as a vector gas and allowed obtaining a plasma. The argon flow rate was kept at 2.8 sccm (sccm stands for Standard Cubic Centimeters per Minute at standard temperature and pressure) and its partial pressure measured using a MKS Baratron gauge was p_{Ar} = 5.32 Pa. HMDSO and argon gas flows were mixed in a buffer chamber before being introduced into the plasma chamber by means of a ring gas injector located in the upper part of the reactor at

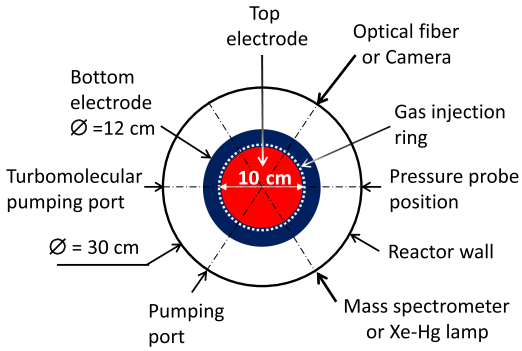

FIG. 1. Schematic top view of the experimental arrangement.

the periphery of the RF electrode. The HMDSO flow rate was adjusted by an OMICRON mass flow controller, switched by an AGILENT pulse generator. This allows introducing the reactive gas by pulses: HMDSO is introduced in the reactor during a t_{on} injection time followed by a t_{off} time. Unless otherwise specified, t_{on} = 2.8 s and the pulsation period, $T = t_{on} + t_{off}$, is 5 s, giving a 0.2 Hz pulse frequency. The total pressure in the discharge increased to 5.93 Pa, weakly oscillating as a function of the HMDSO gas pulses. The maximum accessible HMDSO flow rate was 0.4 sccm, which actually corresponds to a continuous HMDSO gas injection.

Visual observation of the dust cycles was achieved by lighting the discharge with a white light Xe-Hg lamp placed in front of one of the reactor port-holes (Fig. 1). A camera positioned on a port-hole placed at 120° from the lamp axis recorded the light scattered by the particles.

Mass spectrometry (MS) was the main characterization technique used in this work to follow the temporal evolution of the chemical composition of the plasma. The mass spectrometer was a quadrupole HAL EQP 1000 model supplied by Hiden Analytical which offers a 0-300 amu m/z range and also allows positive and negative ion detection. The mass spectrometer was evacuated by a turbomolecular pump. The MS probe head was positioned at a port-hole on the reactor wall (Fig. 1). Species diffused from the plasma into the spectrometer through an aperture of 100 μm in diameter. The mass spectrometer was fitted with an ionization chamber for sampling both neutral (by electron impact) and charged species. To obtain the relative intensities of the neutral species the kinetic energy of the electrons in the MS head was kept at 20 eV. For charged species, specific detection modes were used to collect ions coming from the plasma. The time evolution of the discharge optical emission spectrum (OES) in the 370-800 nm wavelength range was simultaneously recorded with the mass spectrum. The discharge glow emission was captured by an optical fiber positioned 5 mm above the bottom electrode. The optical fiber was connected to a PRINCETON Acton advanced 2500A analyzer.

III. RESULTS

Under the experimental conditions described above, successive cycles of dust generation and disappearance are observed as long as HMDSO is introduced in the discharge. Pseudocolor images taken at different times in a cycle were obtained using the Xe-Hg lamp set-up and are presented in Fig. 2. As discussed in a previous work,[4] the cyclic dust phenomenon is closely related to the experimental conditions, mainly through the RF power and the HMDSO injection time. Under the experimental conditions of Fig. 2 (RF power P = 40 W, Ar flow rate: 2.8 sccm, Ar pressure: 5.32 Pa; HMDSO: t_{on} = 4 s over a period of 5 s) the dust cloud almost completely fills in the reactor in 70 s after the beginning of HMDSO injection (Fig. 2(b)). Only the cathode sheath is free of dusts. Appearance of a void between the border of the cathode sheath (Fig. 2(c)) and the dusty plasma region during the particle growth is observed at each cycle. The asymmetric shape of the void and its position, shifted towards the RF electrode, are due to the asymmetric nature of the RF discharge in this experiment. This is consistent with the large ion flux directed towards the RF electrode and the void can be explained by ion drag force on dust particles. This behavior raises questions about

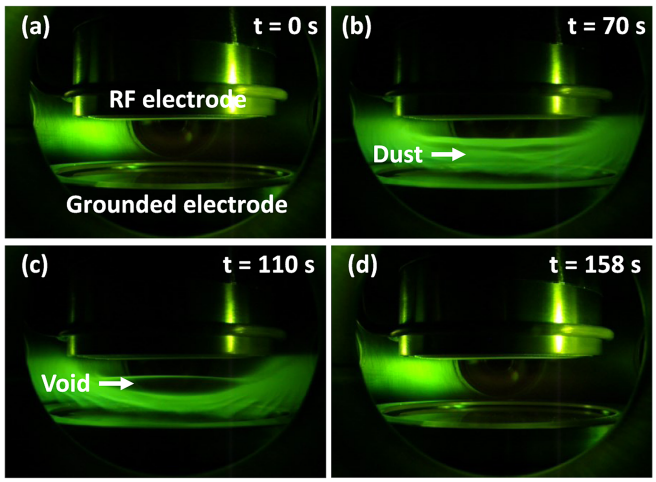

FIG. 2. Time evolution of the dust cycle shown in pseudocolor images. It was obtained by lighting the discharge with a white light. Axially-asymmetric RF discharge in HMDSO-Ar mixture, RF power P = 40 W, Ar flow rate: 2.8 sccm, argon pressure: 5.32 Pa; HMDSO: t_{on} = 4 s over a period of 5 s, in a) t = 0 s (beginning of HMDSO injection in argon discharge), b) t = 70 s, c) t = 110 s, d) t = 158 s. Period of the dust cycle, T_{dust} = 150 s.

plasma sustaining conditions in different locations of the discharge (electron temperature, density of the ionized species, different processes of gain/loss of charged particles, *etc*.). The picture taken after 158 s (Fig. 2(d)) shows that the plasma gets back to its dust-free initial state (Fig. 2(a)). The duration of the dust formation/disappearance cycle under these experimental conditions is T_{dust} = 150 s.[4]

A. Mass spectrometry detection of neutral species

Before analyzing the temporal evolutions of some discharge by-products, it is important to get a global picture of the mass spectrum of the HMDSO-Ar gas mixture. The mass spectrum of the neutral species is presented in Fig. 3 and Fig. 4 with the plasma respectively switched off and on. With the plasma turned off, the main peak corresponds to Ar^+ (m/z = 40 amu) and the main dissociative ionization product of the HMDSO molecule is $Si_2O(CH_3)_5^+$ (m/z = 147 amu, HMDSO-15). The peak at m/z = 162 amu corresponding to the simple ionization of the monomer (e.g. $Si_2O(CH_3)_6^+$) exhibits a very low relative intensity: less than 0.5% of $Si_2O(CH_3)_5^+$ ion (m/z 147 amu). This result confirms the strong instability of HMDSO molecular ion as already reported by other authors.[21,22] Thus, $Si_2O(CH_3)_5^+$ ion intensity will be considered as an image of the HMDSO concentration in

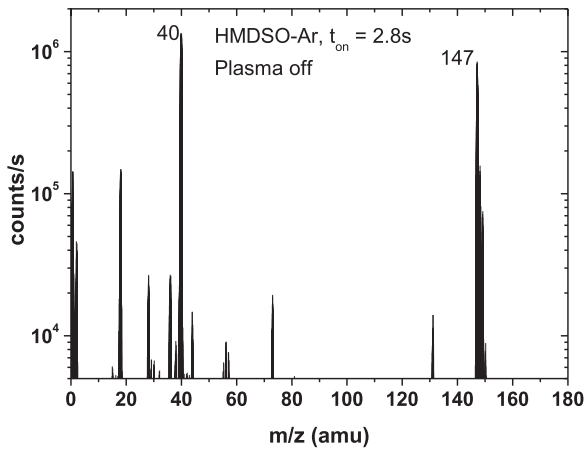

FIG. 3. Mass spectrum of HMDSO-Ar gas mixture. (p_{Ar} = 5.32 Pa, t_{on} = 2.8 s, T = 5 s). RF discharge off. Spectrum obtained during scan time of 1 min.

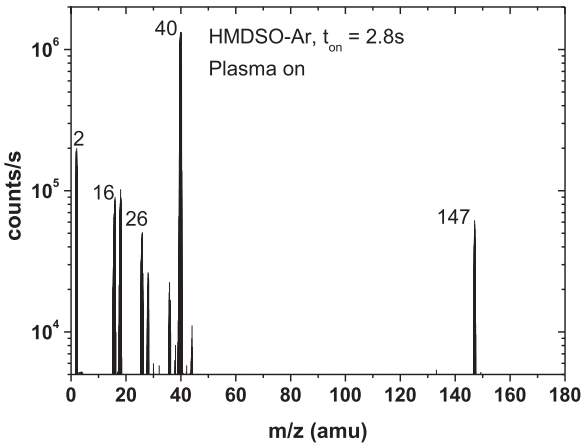

FIG. 4. Mass spectrum of the neutral products in HMDSO-Ar gas discharge. (p_{Ar} = 5.32 Pa, t_{on} = 2.8 s, T = 5 s, P = 30 W). Spectrum obtained during scan time of 1 min as in Fig. 3.

this work. Small amount of HMDSO ion fragments at nominal masses m/z = 73 amu ($Si(CH_3)_3^+$) and m/z = 131 amu ($Si_2OC_4H_{11}^+$), m/z = 2 amu (H_2^+) and some pollutants at m/z = 18 amu (H_2O), m/z = 28 amu (N_2) and m/z = 36 amu were also detected. All these results are in accordance with Basner *et al.*[21]

When the gas discharge is ignited (Fig. 4), a strong decrease of $Si_2O(CH_3)_5^+$ (m/z 147 amu) related to the HMDSO decomposition in the plasma is observed on the mass spectrum. The fragmentation rate, defined as:

$$\tau_f\,[\%] = \frac{I^{off}_{m/z\,147} - I^{on}_{m/z\,147}}{I^{off}_{m/z\,147}} \times 100, \tag{1}$$

where $I^{off}_{m/z\,147}$ and $I^{on}_{m/z\,147}$ are the relative intensities of $Si_2O(CH_3)_5^+$ (m/z 147 amu) when the plasma is off and on, respectively, reaches 95 %. It suggests that even at low discharge power (P = 30 W), HMDSO is very efficiently dissociated in the plasma. Significant peaks at nominal masses m/z = 2 amu, m/z = 16 amu and m/z = 26 amu, respectively assigned to H_2, CH_4 and C_2H_2, are observed in accordance with Alexander *et al.*[22] Neutral Ar atoms (m/z = 40 amu) are also detected. Due to the limit of the mass spectrometer, it was not possible to observe species with nominal mass above 300 amu. Table I gives the direct-ionization rate constants of CH_4, C_2H_2 and HMDSO for the 20 eV energy of incident electrons in the ionization head of the mass spectrometer. CH_4 direct ionization is less favorable than that of C_2H_2 and $Si_2O(CH_3)_6$. The highest intensity of CH_4 peak compared to C_2H_2 peak suggests that in our plasma conditions HMDSO fragmentation leads preferentially to CH_4 formation.

The peaks corresponding to $Si_2O(CH_3)_5^+$ (m/z = 147 amu, HMDSO-15), $C_2H_2^+$ (m/z = 26 amu), and CH_4^+ (m/z = 16 amu) were followed as a function of time (Fig. 5). On a short time-scale, oscillations which periodicity corresponds to that of the HMDSO pulsation (5 s) are observed.

TABLE I. Data for direct ionization of CH_4, C_2H_2 and HMDSO.

Species	m/z	Ionization energy (eV)	Cross section at 20 eV (cm^2)	Rate constant at 20 eV (cm^3/s)
CH_4	16	12.6	0.7×10^{-16}[a]	1.9×10^{-8}
C_2H_2	26	11.4	1.7×10^{-16}[b]	4.5×10^{-8}
$Si_2O(CH_3)_6$	162	8.8	13.4×10^{-16}[c]	35.5×10^{-8}

[a]Reference 23.
[b]Reference 24.
[c]Reference 21.

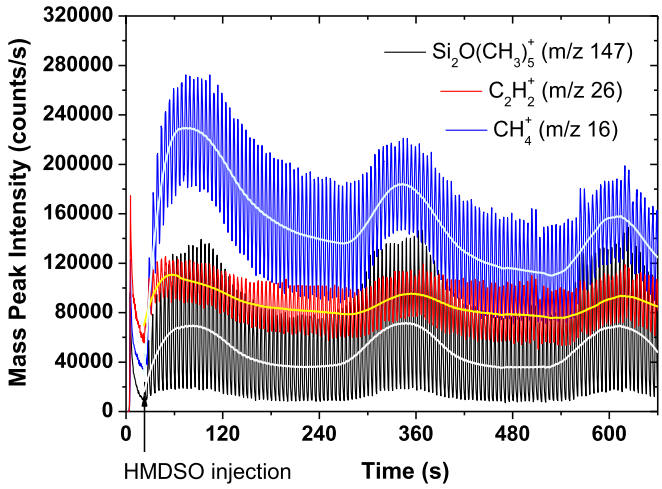

FIG. 5. Time evolution of the mass peaks of m/z 147 amu (HMDSO-15), m/z 26amu (C_2H_2), m/z 16amu (CH_4). (p_{Ar} = 5.32 Pa, t_{on} = 2.8 s,T = 5 s, P = 30 W). The temporal spectra were obtained in profile analysis at fixed mass for each mass peak. The arrow indicates the beginning time of the HMDSO injection. The white and yellow curves are averaged values.

The averaged values shown in Fig. 5 (white or yellow curves) allows following the concentration evolution on longer time-scale. They were obtained by Savitzky-Golay smoothing procedure with polynomial order of 3, as all the other averaged curves shown afterwards. Immediately after the first introduction of HMDSO in the argon discharge ($t_{HMDSOstart}$ = 22 s, shown by an arrow in Fig. 5), the $Si_2O(CH_3)_5^+$ fragment concentration rises (Fig. 5 in black curve). A maximum is reached at t = 76 s, *i.e.* 54 s after the initial injection of HMDSO. Then it decreases reaching a plateau at t = 168 s which lasts until t = 268 s. This phenomenon is repeated with a period T_{dust} = 260 s. CH_4 and C_2H_2 show the same temporal behavior as HMDSO, although the intensity fluctuations of C_2H_2 are less pronounced. This periodic behavior lasts as long as the HMDSO is pulsed in the discharge. These mass spectrometry measurements of neutral by-products confirm both the very low and high frequency oscillations of the discharge which were previously reported through OES measurements.[4]

Methane and acetylene are the two reactive gases usually used for studying carbonaceous dust particles growth in reactive plasmas.[8–12] Acetylene is considered as the precursor of dust particles in hydrocarbon plasmas.[10] The presence of a large amount of C_2H_2 in our spectra suggests an important role of acetylene in dust formation in HMDSO-Ar plasmas. In our case, sputtering of the organosilicon which is deposited from HMDSO species on the RF silver electrode might also play a role.

Figure 6 simultaneously shows the time evolution of the argon emission line at 750.4 nm (the most intensive line in the optical emission spectrum) and the mass peak of $Si_2O(CH_3)_5^+$. It was shown in the literature that the optical emission spectrum of dusty plasmas is modulated by the dust formation/disappearance cycle.[4,10,18,19] In our previous work, we have shown that the oscillations of the Ar emission lines in HMDSO-Ar RF discharges is directly related to the presence of dust particles.[4] Indeed, it was demonstrated that enhancement of the Ar lines emission is related to dust formation whereas the reduction of these emissions corresponds to disappearance of the dust particles from the discharge. A very similar but opposite trend is observed for the $Si_2O(CH_3)_5^+$ MS peak obviously directly related to HMDSO amount; its intensity is lower when the dusts form and higher when they disappear.

In addition, on a shorter time scale (Fig. 6(b)), *i.e.* during one period of HMDSO injection, the concentration of HMDSO and the intensity of the argon emission line are also in anti-phase. This indicates modulation of the plasma parameters over each pulse. Moreover, instability on the dust cloud was observed at the end of the dust cycle which can be considered at the origin of void creation when the dust size is enlarged, further provoking an expansion/contraction of the void with a 5 s pulsation.

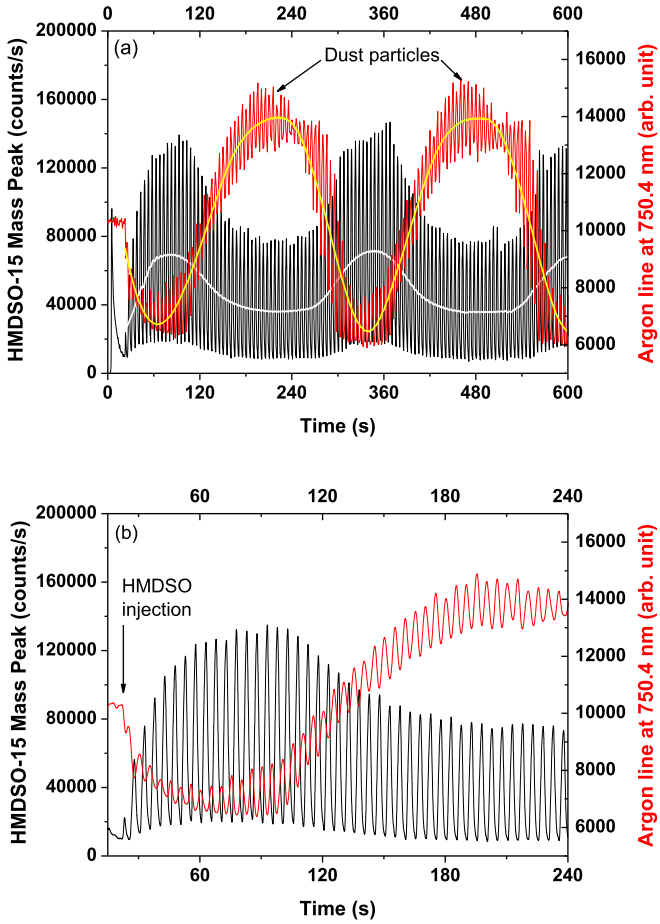

FIG. 6. (a) Time variations of the mass peak m/z 147amu((HMDSO-15)$^+$, black line), and of the argon emission line at 750.4 nm (red line) (p_{Ar} = 5.32 Pa; HMDSO injection time t_{on} = 2.8 s over a period T = 5 s, P = 30 W); (b) Anti-phase behavior of HMDSO-15 (m/z 147 amu) and argon emission line at 750.4 nm on short time-scale.

The above results indicate a clear change in the discharge behavior upon HMDSO injection, inducing important modifications of the plasma parameters. For the time variation of the averaged value of emission lines, it was recently confirmed by Trace Rare Gases Optical Emission Spectroscopy (TRG-OES) measurements that the intensity increase of argon emission lines in our RF discharge reflects an increase of the electron mean energy within the dusty plasma with respect to that energy in the absence of dusts.[19] The increase with time of the electron energy and the corresponding decrease of the electron density during growth of nanoparticles is consistent with the necessity to balance the electron loss due to attachment of low-energy electrons in the fast coagulation phase in accordance with α–γ' transition. To sum up, HMDSO and its neutral by-products follow an anti-phase variation with the cyclic presence of dust particles in the discharge. The decrease of HMDSO averaged amount and that of its by-products during dusty plasma formation indicate a more important dissociation of HMDSO which may favor dust growth and deposition.

B. Molecular hydrogen formation – a specific behavior

Molecular hydrogen is the only neutral species in the plasma that does not obey cyclic behavior. Several studies reported in the literature show that the molecular hydrogen efficiently blocks the positive and negative ion polymerization pathways in hydrocarbon plasmas.[25] Increase of the quantity of H_2 leads to a decrease of the abundancies of high-order hydrocarbon ions. In order to elucidate the role of H_2 in the discharge behavior and its relation with the cyclic phenomenon of dust formation/disappearance, and to complete the results on the neutral species, two sets of additional

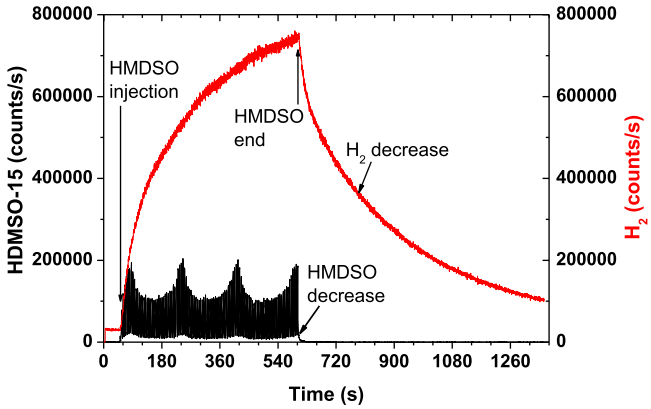

FIG. 7. Time variation of the mass peak m/z 147 amu (HMDSO-15, black line), and of the mass peak m/z 2 amu (H_2, red line) (p_{Ar} = 5.32 Pa, t_{on} = 2.8 s, T = 5 s, P = 30 W).

experiments were carried out. First, simultaneous evolution in time of the mass spectra of HMDSO amount and molecular hydrogen production were recorded. Then the relation between H_2-presence in the discharge and the atomic hydrogen production was analyzed by optical emission spectroscopy (next Section).

The temporal variations of HMDSO and H_2 in the argon discharge before the HMDSO injection, during it, and after the end of HMDSO pulsed injection are shown in Fig. 7. Immediately after the beginning of HMDSO pulsed injection, the periodic variation of HMDSO, on both long- and short-time scales, begins as shown in Fig. 7. The H_2 production however does not follow the periodic phenomenon observed for HMDSO and its by-products (Fig. 5). The amount of molecular hydrogen continuously increases up to saturation (Fig. 7) and holds much higher relative contribution compared to all HMDSO by-products. Once the HMDSO injection in the argon discharge is stopped, a quite rapid fall of the HMDSO density is observed while the H_2 decay is very slow. It takes more than 15 minutes for H_2 to get back to its initial value. The source of H_2 production might be twofold: H-atomic recombination at the surfaces (reactor walls and dust) and bombardment of Ar^+ ion over the SiOC:H deposited film on the RF powered electrode. Indeed, application of pure argon plasma on previously created plasma deposit from HMDSO leads to H_2 production. Nevertheless, a very slow H_2 removal after the end of HMDSO injection and also after the discharge extinction was observed. This H_2 accumulation is most likely related to low H_2 pumping efficiency in the reactor and in the mass spectrometer.

C. Role of atomic hydrogen in the formation/disappearance dust cycle

Figure 8 represents the evolution of the H_α line ($\lambda = 656.28$ nm) and of a close in wavelength argon emission line ($\lambda = 696.54$ nm) as a function of time. First, the time variation of the two spectral lines is quite different even though the oscillation behavior is common to both spectra. Second, the atomic hydrogen production (Fig. 8) does not follow the molecular hydrogen production (Fig. 7). These observations reveal that the production of atomic hydrogen is rather related to the HMDSO decomposition in the discharge and not to a simple H_2 dissociation. Indeed, the intensity of H_α emission line is synchronized with the pulsed injection and the presence of HMDSO in the discharge while the argon emission line dominates when the amount of HMDSO is low, as already discussed. It also indicates that the increase of atomic hydrogen is observed during the dust particle disappearance stage. The question of the key role of atomic hydrogen on the growth mechanisms of dust particles in acetylene plasma has been raised and discussed by Winter *et al.*[10] The introduction of large amount of atomic hydrogen in acetylene plasma quickly inhibits the production of dust particles. It can be supposed in our case that the cyclic production of atomic hydrogen reduces the formation of dust particles. If one assumes formation of dust particles in HMDSO-Ar discharge based on negative ion formation scheme as in hydrocarbon or silane plasmas,[9,15,25] their reduction in presence of atomic hydrogen is due to the instability of the anions like for the very unstable acetylene anion which

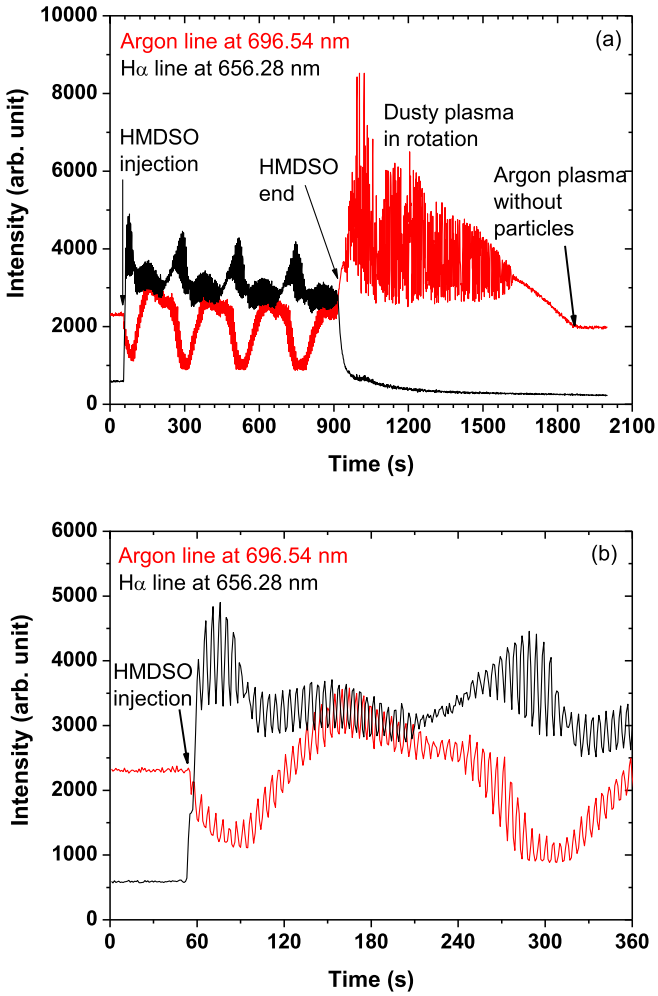

FIG. 8. (a) Temporal evolution of argon line (696.54 nm) and H_α line (656.28 nm) (p_{Ar} = 5.32 Pa, t_{on} = 2.8 s, T = 5 s, P = 30 W). (b) Zoom over the first cycle.

quickly dissociates to C_2H^- and then following the reaction:

$$C_2H^- + H \rightarrow C_2H_2 + e \quad (2)$$

acetylene reformation is achieved.[26,27] The same reaction pathway can apply to the destruction of large masses anions by reactions with H-atoms. Consequently, the plasma dust nucleation could be blocked for a while at the end of the dust cycle. However, the main factor for disappearance of dust particles from the plasma remains the action of various forces (gravity, ion drag, *etc.*) which become dominant when the particle size is increased.

The atomic hydrogen variation in the discharge reveals modification of the discharge behavior in terms of electron temperature and density and inhibition of dust particles. Indeed, the increase of H_α emission is observed just after the beginning of HMDSO injection when the discharge passes from pure argon plasma to HMDSO-Ar mixtures with no dust (Fig. 8(b)). It means that the H-presence is not related to the dust presence but rather to a change in the plasma kinetics. We will get back to this aspect later on when the charged species in the plasma are discussed.

It is worth mentioning the anomalous behavior of Ar-line intensity after the end of HMDSO injection (Fig. 8(a)). It indicates strong instabilities of the energetic conditions in the discharge due to the presence of dust particles and their progressive escape from the reactor. Visually the recorded Ar-line instability is accompanied by rotation of the dust cloud around the smaller electrode in the sheath region where the mean potential drop is high. The dust particles are trapped in this region and

their escape from the discharge is gradual with more regular rotation when their density decreases (t = 1500 – 1620 s in Fig. 8(a)). The Ar-line intensity gets back to its initial value, characteristic to the pure Ar-discharge, when all dust particles disappear from the plasma. Observation of such instabilities was reported for capacitively-coupled RF dusty plasmas where the precursor for dust formation is sputtered material from the electrode. Given their characteristic motion these instabilities were called carousel instabilities.[28,29] The same mechanism can be suggested for our experiment. As the feeding of the reactive gas is stopped, only sputtering of organosilicon material from the powered electrode takes place to provide dust precursors and induce carousel instabilities.

D. Mass spectrometry detection of positive ions in the RF discharge during the dusty plasma production

At this point it seems necessary to make an assessment of the nature and the relative amounts of ions present in the HMDSO-Ar discharge. The recorded mass spectrum of positive ions from the plasma is shown in Fig. 9. It indicates the following species: H_3^+ (m/z = 3 amu), CH_3^+ (m/z = 15 amu), $C_2H_2^+$ (m/z = 26 amu), Ar^+ (m/z = 40 amu), ArH^+ (m/z = 41 amu), $SiH(CH_3)_2^+$ (m/z = 59amu), $Si(CH_3)_3^+$ (m/z = 73 amu), $Si_2OH(CH_3)_4^+$ (m/z = 133amu) and $Si_2O(CH_3)_5^+$ (m/z = 147 amu). In addition, some very low quantities of $Si_2O(CH_3)_6^+$(m/z = 162 amu) and of heavier ions (nominal masses m/z = 193 amu, 205 amu, 207 amu, 221 amu) were detected. Positive ions with higher nominal masses might also be present in the discharge as reported for HMDSO plasmas.[22] They cannot be recorded in our case due to the limitation of the used mass spectrometer (up to m/z = 300 amu). No negatively charged species were detected. The limitation here does not stem from the capability of the mass spectrometer as it is adapted also for detection of negatively charged species. It is rather a consequence of the trapping of negative ions in the plasma potential and of the low stability of the created anions from HMDSO by-products. For example, the acetylene anion ($HCCH^-$) is found to be very unstable with respect to auto-detachment process.[26]

Under the studied plasma conditions ArH^+ and $Si_2O(CH_3)_5^+$ are the dominant ions. The amount of ArH^+ ion largely overcomes the Ar^+ one. This effect is due to the very fast conversion rate (large cross section) for Ar^+ in the energy range 0.01 – 0.1 eV following the reaction:[30,31]

$$Ar^+ + H_2 \rightarrow ArH^+ + H. \quad (3)$$

The observed accumulation of H_2 in the HMDSO-Ar plasma (Fig.7) is rather favorable for the creation of ArH^+ ions. The effect of molecular hydrogen on the argon plasma density was already studied by other authors showing that the presence of H_2 leads to anomalous loss of argon atomic ions.[32,33]

1. Temporal variation of the Ar^+ ion

Experimental observations on the behavior of Ar^+, already reported in the literature, are well confirmed by our study (Fig. 10) where Ar^+ ion density before and during HMDSO injection is

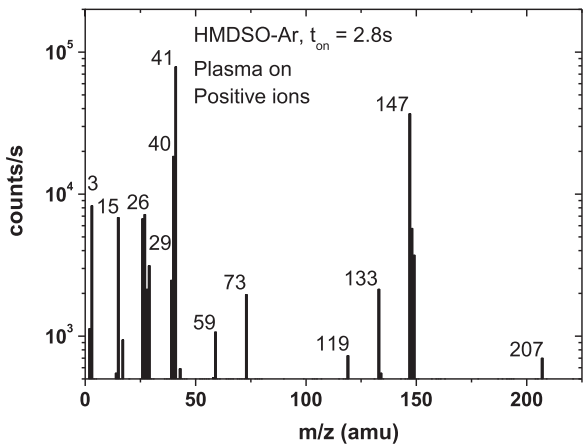

FIG. 9. Mass spectrum of positive ions in HMDSO-Ar gas discharge (p_{Ar} = 5.32 Pa, t_{on} = 2.8 s, T = 5 s, P = 30 W).

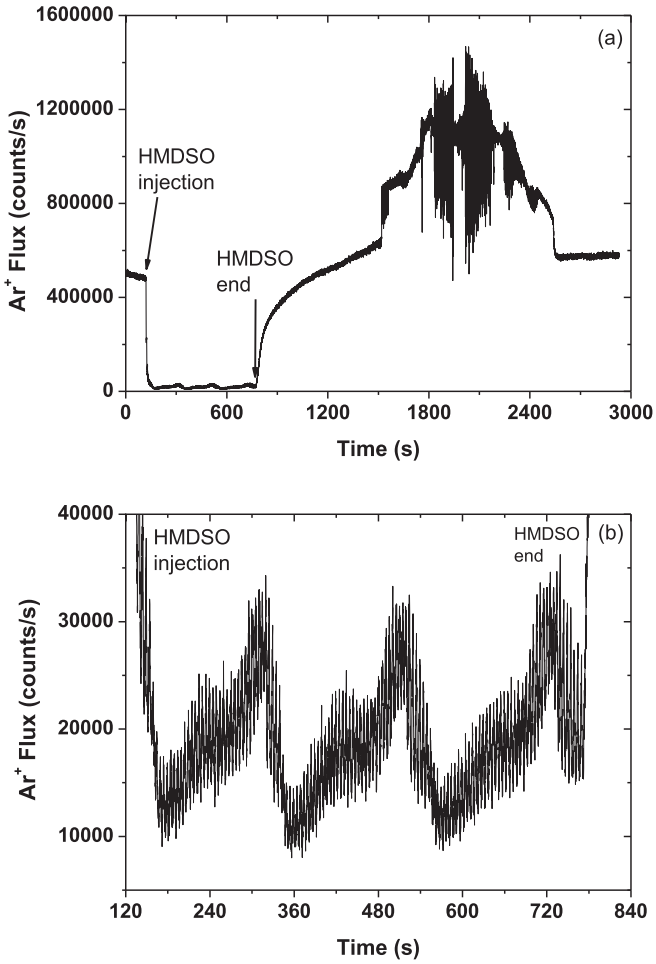

FIG. 10. (a) Variation of Ar^+ escaping the discharge before and after HMDSO injection detected by mass spectrometry; (p_{Ar} = 5.32 Pa, t_{on} = 2.8 s, T = 5 s, P = 30 W); (b) Zoom in the dusty plasma part.

followed. Before HMDSO introduction in the discharge the argon ion flux is approximately 5×10^6 counts/s whereas when the HMDSO introduction starts, the positive argon flux is reduced and almost stabilized at low relative intensity (lower than 3×10^4 counts/s). However, the important decrease of Ar^+ ion flux is not directly related to the periodic phenomena due to the dusty plasma formation although a cyclic phenomenon is also observed to the lowest values on Ar^+ ion population (Fig. 10(b)). Let us note the increase of Ar^+ during the formation stage of dust particles just before their disappearance (Fig. 10(b)). Note also the fluctuations in Ar^+ production after the end of HMDSO introduction. This indicates the presence and the escape of dust particles from the pure argon discharge (Fig. 10(a)). The observed difference between Fig. 10(b) and Fig. 8(a) in the delay of fluctuations is related to the moment of HMDSO end during the cycle of dusty plasma production. Indeed, for the experiment presented in Fig. 8(a) the HMDSO injection was stopped during dust presence in the discharge, whereas it was done when no dust was observed in the plasma in Fig. 10(b). This suggests that the sputtering of carbonaceous film deposited on the powered electrode also takes part in the dusty plasma formation.

2. Temporal variation of the ArH^+ ion

The temporal variation of ArH^+ ions is followed as a function of HMDSO injection as shown in Fig. 11. A periodic phenomenon rather similar to those of the Ar emission lines (Fig. 5) and of argon ions (Fig. 10(b)) is observed for ArH^+ ions. A positive drift of the mean amplitude is detected, probably due to a higher ArH^+ formation over time because of H_2 accumulation in the reactor (Fig.7).

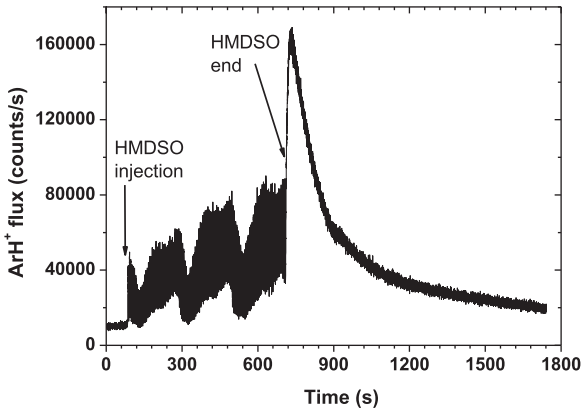

FIG. 11. Variation of positive ion flux of ArH^+ before and after HMDSO injection (p_{Ar} = 5.32 Pa, t_{on} = 2.8 s, T = 5 s, P = 30 W).

After ending HMDSO injections, an abrupt increase of ArH^+ amount is observed. This increase cannot be related to the increase of H_2 amount, which actually starts to decrease at that time, but corresponds to the increase of Ar^+ ion concentration. Indeed, when the discharge is no more supplied with HMDSO, electron interactions with the residual reactive gas become limited. Consequently, the rate of direct ionization increases enhancing Ar^+ production. The conversion process of Ar^+ atomic ions into ArH^+ molecular ions becomes then the main loss channel for Ar^+ atomic ions, *i.e.* the main gain channel for ArH^+ ions. It leads to an instantaneously strong increase of ArH^+ as H_2 is still quite abundant (Fig. 7). Compared to other Ar^+ loss channels ((1) ambipolar diffusion to the reactor walls, (2) 3-body recombination in volume, and (3) conversion into argon molecular ions Ar_2^+) the (4) conversion of Ar^+ into ArH^+ happens with a frequency of at least two orders of magnitude higher. The decrease of ArH^+ is due to the H_2 slow disappearance from the operating system. Table II summarizes the different loss channels and frequencies of Ar^+ ions. The calculations of the reaction frequencies are given in the Appendix.

Although H_2 is clearly produced in the plasma reactor and the evolutions of Ar^+ and ArH^+ are essentially related to Reaction 4 in Table II, one should bear in mind that a large amount of H_2 is accumulated in the mass spectrometer due to the difficulty of H_2 turbo molecular pumping. It means that the measured ArH^+ density can be overestimated with respect to the Ar^+ density in the discharge.

3. Temporal variation of the $Si_2O(CH_3)_5^+$ ion

Changes in the concentration of $Si_2O(CH_3)_5^+$ ion over time show an increase during the increase of the averaged HMDSO parent monomer. They are consistent with the global increase of the ion

TABLE II. Channels and frequencies for loss of Ar^+ atomic ions.

N°	Reaction	Rate coefficient	Frequency
1	Ambipolar diffusion $-D_a$	$D_a = 8.3 \times 10^4$ cm^2/s[a]	$\nu_{Da} = 5.3 \times 10^2$ s^{-1}
2	3-body recombination $Ar^+ + e + e \rightarrow Ar + e$	$\rho_{tr} = 8.75 \times 10^{-27} (T_e$ [eV])$^{-9/2}$ cm^6/s[b]	$\nu_{tr} = 8.7 \times 10^{-8}$ s^{-1}
3	Conversion into molecular ions $Ar^+ + Ar + Ar \rightarrow Ar_2^+ + Ar$	$k_{1\text{-}MI} = 2.25 \times 10^{-31} (T_g$ [K]/300)$^{-0.4}$ cm^6/s[c]	$\nu_{1\text{-}MI} = 3.7 \times 10^{-1}$ s^{-1}
4	Conversion into molecular ions $Ar^+ + H_2 \rightarrow ArH^+ + H$	$k_{2\text{-}MI} = 9.2 \times 10^{-10}$ cm^3/s[d]	$\nu_{2\text{-}MI} = 6.6 \times 10^5$ s^{-1}

[a]Reference 34.
[b]Reference 35.
[c]Reference 36.
[d]Reference 31.

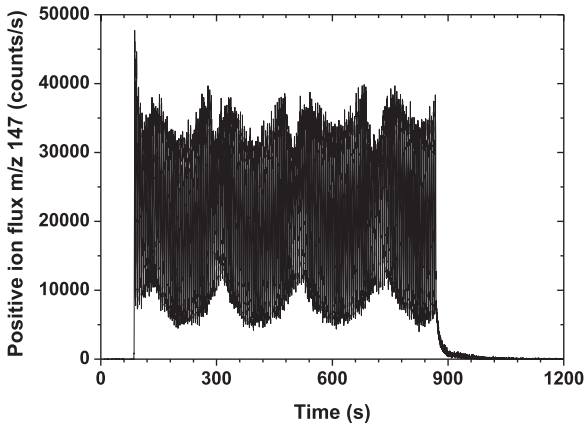

FIG. 12. Variation of positive ion flux of $Si_2O(CH_3)_5^+$ before and after HMDSO injection (p_{Ar} = 5.32 Pa, t_{on} = 2.8 s, T = 5 s, P = 30 W).

density. End of HMDSO injection in the discharge leads to a fast disappearanceof $Si_2O(CH_3)_5^+$ ion (Fig. 12).

4. Comparison of the temporal variations of the main positive ions in the discharge

The relative contributions of the main ions in the discharge are compared in Fig. 13. The temporal evolution of the total positive ion flux shows an increase during the dusty plasma formation with a maximum just before the dust disappearance (Fig. 13(a)). At short time scale (5 second period for the HMDSO injection, Fig. 13(b)), the production of $Si_2O(CH_3)_5^+$ positive ions prevails during HMDSO injection (t_{on}). When injection of HMDSO is stopped (t_{off}) Ar^+ and ArH^+ are the dominant ions. Moreover Ar^+ and ArH^+ ions behave similarly over time. These results confirm that the discharge kinetics is controlled by the production of $Si_2O(CH_3)_5^+$ ion during HMDSO time "on" (t_{on}), while it is dominated by Ar and the HMDSO by-products during time "off" (t_{off}).

IV. CONSISTENT DESCRIPTION OF THE OBSERVED PROCESSES - ATTEMPT

Consistent description of the observed processes requires considering two major different situations: (*i*) a situation where the plasma maintenance is dominated by electron-HMDSO parent molecule interactions representing the case without dust and (*ii*) a situation where the plasma is controlled by electron-argon atom interactions when the dust is formed in the plasma. Due to the dust presence in the second case the electron temperature is increased in order to compensate the electron attachment on dust nanoparticles. The role of organosilicon ions in the void formation and the following dust disappearance should also be considered.

The large efficiency of HMDSO dissociation by electron impact, with an average electron energy of a few eV for argon plasma (T_{e_ave} = 3.9 eV for the experimental conditions in this work),[19] significantly changes the argon discharge maintenance when this reactive gas is added. For energies below the HMDSO ionization energy (8.8 eV), the dissociation of the HMDSO molecule by electron impact is the dominant process.[21,37] As the bonding energy of the Si–O bond (8.31 eV) is almost twice higher than that of the Si–C bond (4.53 eV), the radical dissociation process induces a dominant production of the neutral radicals $^\circ CH_3$ and $Si_2O(CH_3)_5$ (HMDSO-15). Therefore, further reactions in the chain will be primarily initiated by these two most abundant reactive species produced in the plasma. Due to the important difference between the energy thresholds for ionization of argon (15.76 eV) and for production of the HMDSO fragment ion HMDSO-15 (9.6 eV), the HMDSO dissociative ionization controls the discharge behaviour when the HMDSO concentration is significantly high. One can notice that the ionization energy of HMDSO for the production of $Si_2O(CH_3)_5^+$ is even below the threshold for excitation of the first excited state of the Ar atom (11.548 eV for the $Ar3s^23p^5(^2P^\circ_{3/2})4s$ level). Accordingly, the favorable interactions between electrons and HMDSO are largely involved

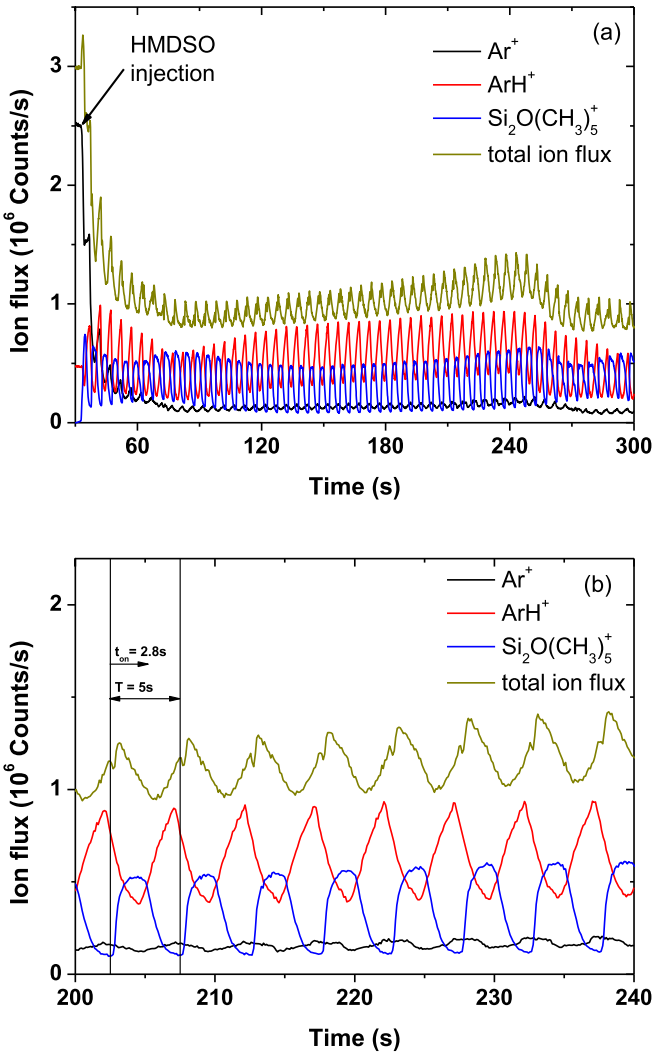

FIG. 13. (a) Relative contributions of the main positive ion fluxes Ar^+, ArH^+ and $Si_2O(CH_3)_5^+$; (p_{Ar} = 5.32 Pa, t_{on} = 2.8 s, T = 5 s, P = 30 W); (b) Zoom in the dusty plasma part.

in the discharge maintenance under the studied experimental conditions during HMDSO injection in the discharge and especially with no dust.

Due to the wide variety of chemical bonds in HMDSO, it can be assumed that the cross sections of vibrational excitations are large. Unfortunately these data are not available in the literature. The assumption made implies that the interactions of HMDSO with the group of electrons belonging to the low part of the electron energy distribution function are predominant. Besides, it has been reported[22,38] that electron attachment is not observed in pure HMDSO or in HMDSO-Ar mixtures. Our attempts to record negative ions in the HMDSO-Ar discharge also failed. Consequently, the interactions between the low-energy electrons and the HMDSO parent molecules would lead to a change in the electron temperature. Indeed, this is the process observed on the argon line intensities (a decrease) at the very beginning of the experiments when the pulsed injection of HMDSO starts (Figs. 6 and 8) and no dust is yet observed. Moreover, as discussed above the dissociative ionization of HMDSO is strong. The recorded in this situation decrease of the argon line intensities is due to the enhanced, by the HMDSO admixture, ionization in the argon discharge. As a consequence, the needed mean energy to sustain the discharge, a quantity proportional to the electron temperature, is lowered. The strong HMDSO fragmentation at that stage, and mainly the produced large amount of C_2H_2, gives the necessary precursors to initiate dust nucleation. The moment at

which the HMDSO by-products start to decrease can be considered as the beginning of the fast coagulation stage of dust formation, as the pulsed HMDSO injection is continued at that time thus, feeding constantly the discharge (Fig. 5). Moreover, this is the same moment at which the argon line intensity starts to increase (Fig. 6), with the later associated with an increase of the electron temperature.[4,19] When the dust starts to induce modifications in the plasma maintenance with an observable impact on the electron energy ↔ electron density settings the size of the nanoparticles is sufficiently large that they can be trapped in the plasma and the dust cloud to become observable (Fig. 2(b)). The strong modulation of both electron density and electron temperature actually indicates the α–γ′ transition in the discharge maintenance. The electron temperature increases in order to compensate the enlarged loss of electrons on the dust and the electron density drops by more than two orders of magnitude, as recently confirmed by TRG-OES for the same HMDSO-Ar discharge.[19]

The decrease of HMDSO by-products during dusty plasma formation indicates also an even more important fragmentation of the HMDSO parent molecule as it happens in conditions of constantly increasing electron temperature. The increase of electron temperature can favor a larger HMDSO dissociation even if the electron density significantly decreases. Another possibility would be that the negatively charged particles strongly react with organic compounds. Nevertheless, it is difficult to conclude on this last idea without more evidences.

The production of larger amount of active species favors the dust growth by accretion. This corresponds to the second situation that we have mentioned earlier. Looking on the time evolution of the positive ions (Fig. 13) one can see that the ArH^+ and $Si_2O(CH_3)_5^+$ (HMDSO-15) are in anti-phase. Moreover, the electron-argon atom interactions prevail as shown in Fig. 6 and Fig. 13, through the increased line intensity of the Ar-excited species and the predominant amount of ArH^+ ions, respectively. The intensity of the argon lines decreases when the dust starts to disappear from the discharge. It is representative of a decrease of the electron temperature and an increase of the followed HMDSO by-product (Fig. 6). It indicates a return to the situation where the plasma is rather sustained by interactions of electrons with HMDSO parent molecules. This actually represent the reverse transition in the discharge maintenance, *i.e.* γ′–α transition that happens in the end of each cycle of dust formation/disappearance. On the other side, the injected HMDSO contributes to the formation of heavy positive ions ($Si_2O(CH_3)_5^+$, m/z = 147 amu, Fig. 13). It is now generally accepted that the void appearance and its extension is adequately explained by the ion drag force, which becomes stronger than the opposing Coulomb force once the particle size reaches a critical value. The dust-free region develops when the ionization rate is increased and the ion flow that pushes particles outward the discharge is enlarged.[13,16] In our case, the significant creation of heavy positive ions ($Si_2O(CH_3)_5^+$ m/z = 147 amu) can additionally enhance the ion drag force exerted on the dust particles, repelling them to the wall and inciting their disappearance. The observation of the void beat at the same frequency as the frequency of the HMDSO injection (rapid oscillations) suggests a role of HMDSO injection on the dust instabilities through the $Si_2O(CH_3)_5^+$ ions. A point that supports such statement is that during each HMDSO pulse the $Si_2O(CH_3)_5^+$ becomes the major ion in the plasma, compared to Ar^+ and ArH^+ ions (Fig. 13(b)) inducing instabilities in the dust cloud and void creation. The HMDSO admixture (t_{on} = 2.8 s over 5 s corresponding to HMDSO flow of only 0.224 sccm) is small compared to the argon flow (2.8 sccm) to induce a ram blow effect. However, the correlation between the void beat frequency and the frequency of HMDSO injection should be further investigated. Based on the above observations it can be concluded that the void creation marks the beginning of the γ′–α transition in the discharge maintenance during cyclic production of dust with pulsed injection of HMDSO in argon discharge.

As far as the H-atom production was detected when the dust disappears from the plasma at each cycle or during the transition from pure argon plasma to HMDSO-Ar plasma at the very beginning of the experiment its role can be associated only with the nucleation stage of dust formation. Indeed, presence of H-atoms can inhibit the active carbon promoter (C_2H^- or C^-) of dust nucleation[10,25] and consequently delays the dust growth. Once the HMDSO injection is stopped, the H-atoms are quickly evacuated from the discharge and have no additional effect on the dust (Fig. 8(a)). The H-atoms do not influence the dust which is created after sputtering of previously deposited material on the electrodes.

V. CONCLUSIONS

As already reported in a previous work and confirmed here, the pulsed injection of HMDSO in argon RF discharge induces cyclic formation/disappearance of successive generations of dust nanoparticles at very-low-frequency oscillations. The periodic formation of dusty plasma is inversely related to the HMDSO injection time over a fixed pulse period. The various processes put in play are revealed in this work by progressive in time mass spectrometry in correlation with the discharge glow evolution analyzed by optical emission spectroscopy. A large amount of C_2H_2, considered as promoter of dust nucleation in hydrocarbon plasmas, is found as by-product of the HMDSO fragmentation supporting the hypothesis of dust growth mechanism based on negative ions trapped in the plasma potential. The α–γ′ transition in the discharge maintenance is observed for each cycle at the stage of dust formation whereas the reverse transition, *i.e.* γ′–α transition, occurs at the end of the cycle when the dust disappears from the discharge. As already described by other authors, the α–γ′ transition is related to the beginning of the fast coagulation phase of the very first proto-particles. When the agglomeration phase starts, the electron attachment becomes very important, inducing a strong increase of the electron temperature. The start of the agglomeration phase can be associated in our study with the beginning of strong fragmentation of the main HMDSO by-products: HMDSO-15, CH_4 and C_2H_2. The beginning of the reverse transition, *i.e.* γ′–α, corresponds to a drop of the electron temperature and as a visible aspect, to the creation of a void in the dust cloud. The creation of a void is induced by dust particles instabilities due to the drag force exerted by the HMDSO ions with large masses. The discharge is dominated by $Si_2O(CH_3)_5^+$ ions when dust starts to disappear. This effect is also detected over short time scale representing the frequency of HMDSO injection pulse. Once the void is created, it starts to beat with the same frequency as the frequency of HMDSO injection pulse most likely in relation with the HMDSO ionization and the control of discharge behavior exerted by the $Si_2O(CH_3)_5^+$ ions. Indeed our results show that Ar^+ and ArH^+ ions dominate the discharge maintenance only when the dust nanoparticles are present in the discharge. The observed here complex processes indicate: (*i*) a competition between the electron attachment on dust particles and the interactions of electrons with HMDSO parent molecules for the low-energy group of electrons (<10 eV) to produce both excitation and dissociation of HMDSO, (*ii*) an input of the heavy positive ions ($Si_2O(CH_3)_5^+$, m/z = 147 amu) pushing previously formed bigger dust particles toward the plasma edge thus creating the void in the dust cloud, (*iii*) an H-atomic production which appears an inhibitor of dust promoters delaying the nucleation stage of dust formation. H-atomic production is revealed by optical emission spectroscopy. Its presence is clearly observed during the transition from dusty plasma to plasma with HMDSO-dominant composition without dust nanoparticles.

Further work will be oriented to analysis of the chemical composition of dust nanoparticles and possibilities to identify their size and composition at different moments of the cyclic formation/disappearance process. Apart from the technological aspect aiming at a design of nanocomposite thin layers, the astrophysical interest of generation of cosmic dust analogues will also be explored.

ACKNOWLEDGMENTS

The authors thank C. Joblin (IRAP-OMP, Toulouse) for many useful discussions. This work is financially supported by the Fondation de Coopération Scientifique "Sciences et Technologies pour l'Aéronautique et l'Espace", RTRA-STAE in France, project 3PC keys under Contract N°RTRA-STAE/2014/P/3PCKEYS/01.

APPENDIX: EXPRESSIONS FOR THE COLLISIONAL AND TRANSPORT PROCESSES USED FOR ESTIMATION OF THE REACTION FREQUENCIES OF DIFFERENT CHANNELS OF LOSS OF ARGON ATOMIC IONS

The frequencies of different channels of loss of Ar^+ ions reported in Table II were estimated on the basis of the following assumptions for the electron temperature of T_e = 2.6 eV as measured by TRG-OES[19] and for the electron density of $n_e = 2.7 \times 10^{10}$ cm^{-3} as measured by Langmuir probe technique[39] in an argon capacitively coupled discharge sustained in the same plasma reactor. The gas temperature was taken T_g = 300 K.

1. Ambipolar diffusion

Apart from the drift to the electrodes, at low gas pressures the transport of charged particles to the walls is related to the ambipolar diffusion. The ambipolar diffusion coefficient is calculated on the basis of its relation to the ion mobility with $\mu_{i0Ar+} = 1.52\ cm^2V^{-1}s^{-1}$ at atmospheric pressure and gas temperature 273 K.[34] For a pressure of $p = 5.32$ Pa and $T_g = 300$K the Ar^+ ion mobility reads:

$$\mu_{iAr^+}\left[cm^2/Vs\right] = \mu_{i0Ar^+}\frac{p_{Atm[Torr]}}{k_B 273}\frac{k_B T_{g[K]}}{p_{[Torr]}} = 3.2 \times 10^4 cm^2/Vs. \quad (A1)$$

The ambipolar diffusion coefficient is then:

$$D_A = T_{e[eV]}\mu_{iAr^+[cm^2/Vs]} = 8.3 \times 10^4 cm^2/s, \quad (A2)$$

which defines a diffusion time:

$$\tau_{D_A} = \frac{\Lambda^2}{D_A} = 1.9 \times 10^{-3} s, \quad (A3)$$

with characteristic length of $\Lambda = R/2.4$, accounting for a Bessel profile of the electron density, R is the reactor radius. The frequency is then considered as:

$$\nu_{D_A} = \frac{1}{\tau_{D_A}} = 5.3 \times 10^2\ s^{-1}. \quad (A4)$$

2. 3-body recombination

$$Ar^+ + e + e \rightarrow Ar + e \quad (A5)$$

In general, the 3-body recombination is not a significant process at low gas pressure. According to Ref. 35, the rate coefficient for 3-body recombination is:

$$\rho_{tr}\left[cm^6/s\right] = 8.75 \times 10^{-27}\ (T_e\,[eV])^{-4.5}. \quad (A6)$$

Considering the low electron density in argon capacitively-coupled discharges, the frequency of 3-body recombination is:

$$\nu_{tr} = 8.7 \times 10^{-8}\ s^{-1}. \quad (A7)$$

3. Conversion of argon atomic ions Ar^+ into argon molecular ions Ar_2^+

$$Ar^+ + Ar + Ar \rightarrow Ar_2^+ + Ar. \quad (A8)$$

Processes involving three particles are not of great importance for discharges sustained at low gas pressure. The rate coefficient for conversion of this process is:[36]

$$k_{1-MI}\left[cm^6/s\right] = 2.25 \times 10^{-31}\ \left(T_g\,[K]/300\right)^{-0.4}, \quad (A9)$$

which defines a frequency of:

$$\nu_{1-MI} = 3.7 \times 10^{-1}\ s^{-1}. \quad (A10)$$

4. Conversion of argon atomic ions Ar^+ into molecular ions ArH^+

$$Ar^+ + H_2 \rightarrow ArH^+ + H. \quad (A11)$$

Considering quasi-neutrality principle for charged particles the estimation here is made with the value corresponding to the electron density of pure argon discharge. The density of molecular hydrogen is estimated on the basis of the mass spectrometry measurements considering the relative intensities of the measured values for Ar-atom and H_2-molecular hydrogen (Fig. 4). The accumulation of H_2 in the discharge (Fig. 7) is taken into account which means that the obtained value represents the upper

limit for this process. In the beginning of HMDSO injection in the argon discharge the density of H_2 is an order of magnitude lower which defines the lower limit or this reaction. The rate coefficient of conversion of argon atomic ions Ar^+ into molecular ions ArH^+ reads:[31]

$$k_{2-MI}\left[\mathrm{cm}^3/\mathrm{s}\right] = 9.2 \times 10^{-10}. \quad \text{(A12)}$$

Given our reasoning for the upper limit this process happens with a frequency of:

$$\nu_{2-MI} = 6.6 \times 10^5\ \mathrm{s}^{-1}. \quad \text{(A13)}$$

[1] G. S. Selwyn, J. Singh, and R. S. Bennett, "*In situ* laser diagnostic studies of plasma-generated particulate contamination," J. Vac. Sci. Technol. A **7**, 2758–2765 (1989).
[2] A. Bouchoule and L. Boufendi, "Particulate formation and dusty plasma behaviour in argon-silane RF discharge," Plasma Sources Sci. Technol. **2**, 204–213 (1993).
[3] U. Kortshagen, "Nonthermal plasma synthesis of semiconductor nanocrystals," J. Phys. D: Appl. Phys. **42**, 113001 (2009).
[4] B. Despax, K. Makasheva, and H. Caquineau, "Cyclic powder formation during pulsed injection of hexamethyldisiloxane in an axially asymmetric radiofrequency argon discharge," J. Appl. Phys. **112**, 093302 (2012).
[5] M. Ricci, J.-L. Dorier, Ch. Hollenstein, and P. Fayet, "Influence of argon and nitrogen admixture in HMDSO/O_2 plasmas onto powder formation," Plasma Processes Polym. **8**, 108 (2011).
[6] M. Mikikian, L. Boufendi, A. Bouchoule, H. M. Thomas, G. E. Morfill, A. P. Nefedov, V. E. Fortov, and the PKE–Nefedov team, "Formation and behaviour of dust particle clouds in a radio-frequency discharge: results in the laboratory and under microgravity conditions," New J. Phys. **5**, 19.1 (2003).
[7] M. Cavarroc, M. Mikikian, Y. Tessier, and L. Boufendi, "Successive Generations of Dust in Complex Plasmas: A Cyclic Phenomenon in the Void Region," Phys. Rev. Lett. **100**, 045001 (2008).
[8] E. Kovacevic, I. Stefanovic, J. Berndt, and J. Winter, "Infrared fingerprints and periodic formation of nanoparticles in Ar/C_2H_2 plasmas," J. Appl. Phys. **93**, 2924 (2003).
[9] I. Stefanovic, E. Kovacevic, J. Berndt, and J. Winter, "H_α emission in the presence of dust in an Ar–C_2H_2 radio-frequency discharge," New J. Phys. **5**, 39.1 (2003).
[10] J. Winter, J. Berndt, S.-H. Hong, E. Kovacevic, I. Stefanovic, and O. Stepanovic, "Dust formation in Ar/CH_4 and Ar/C_2H_2 plasmas," Plasma Sources Sci. Technol. **18**, 034010 (2009).
[11] S. Dap, D. Lacroix, F. Patisson, R. Hugon, L. de Poucques, and J. Bougdira, "Agglomeration processes in carbonaceous dusty plasmas, experiments and numerical simulations," New J. Phys. **12**, 093014 (2010).
[12] Ch. Deschenaux, A. Affolte, D. Magni, Ch. Hollenstein, and P. Fayet, "Investigations of CH_4, C_2H_2 and C_2H_4 dusty RF plasmas by means of FTIR absorption spectroscopy and mass spectrometry," J. Phys. D: Appl. Phys. **32**, 1876 (1999).
[13] G. Praburam and J. Goree, "Experimental observation of very low-frequency macroscopic modes in a dusty plasma," Phys. Plasmas **3**, 1212 (1996).
[14] D. Samsonov and J. Goree, "Instabilities in a dusty plasma with ion drag and ionization," Phys. Rev. E **59**, 1047 (1999).
[15] A. A. Fridman, L. Boufendi, T. Hbid, B. V. Potapkin, and A. Bouchoule, "Dusty plasma formation: Physics and critical phenomena. Theoretical approach," J. Appl. Phys. **79**, 1303 (1996).
[16] Ch. Hollenstein, "The physics and chemistry of dusty plasmas," Plasma Phys. Controlled Fusion **42**, R93 (2000).
[17] P. Belenguer, J.-Ph. Blondeau, M. Toogood, A. Plain, A. Bouchoule, C. Laure, and J.-P. Boeuf, "Numerical and experimental diagnostics of rf discharges in pure and dusty argon," Phys. Rev. A **46**, 7923 (1992).
[18] V. Massereau-Guilbaud, I. Géraud-Grenier, J.-F. Lagrange, H. Tawidian, and M. Mikikian, "Electron temperature evolution in a low-pressure dusty RF nitrogen-rich methane plasma," IEEE Trans. Plasma Sci. **41**, 816 (2013).
[19] V. Garofano, L. Stafford, B. Despax, R. Clergeraux, and K. Makasheva, "Cyclic evolution of the electron temperature and density in dusty low-pressure RF plasmas with pulsed injection of hexamethyldisiloxane," Appl. Phys. Lett. **107**, 183104 (2015).
[20] B. Despax and P. Raynaud, "Deposition of 'Polysiloxane' thin films containing silver particles by an RF asymmetrical discharge," Plasma Processes Polym. **4**, 127 (2007).
[21] R. Basner, R. Foest, M. Schmidt, K. Becker, and H. Deutsch, "Absolute total and partial electron impact ionization cross sections of hexamethyldisiloxane," Int. J. of Mass Spectrometry **176**, 245 (1998).
[22] M. R. Alexander, F. R. Jones, and R. D. Short, "Mass spectral investigation of the radio-frequency plasma deposition of hexamethyldisiloxane," J. Phys. Chem. B **101**, 3614 (1997).
[23] Y.-K. Kim, W. Hwang, N. M. Weinberger, M. A. Ali, and M. E. Rudd, "Electron-impact ionization cross sections of atmospheric molecules," J. Chem. Phys. **106**, 1026 (1997).
[24] Y.-K. Kim, M. A. Ali, and M. E. Rudd, "Electron-impact total ionization cross sections of CH and C_2H_2," J. Res. NIST **102**, 693 (1997).
[25] K. De Bleecker and A. Bogaerts, "Detailed modeling of hydrocarbon nanoparticle nucleation in acetylene discharges," Phys. Rev. E **73**, 026405 (2006).
[26] K. M. Ervin, J. Ho, and W. C. Lineberger, "A study of the singlet and triplet states of vinylidene by photoelectron spectroscopy of $H_2C{=}C^-$, $D_2C{=}C^-$, and $HDC{=}C^-$. Vinylidene-acetylene isomerization," J. Chem. Phys. **91**, 5974 (1989).
[27] S. Stoykov, C. Eggs, and U. Kortshagen, "Plasma chemistry and growth of nanosized particles in a C_2H_2 RF discharge," J. Phys. D: Appl. Phys. **34**, 2160 (2001).
[28] M. Mikikian, L. Couëdel, Y. Tessier, and L. Boufendi, "Carousel Instability in a Capacitively Coupled RF Dusty Plasma," IEEE Trans. Plasma Sci. **39**, 2748 (2011).
[29] M. Mikikian, H. Tawidian, and T. Lecas, "Merging and splitting of plasma spheroids in a dusty plasma," Phys. Rev. Lett. **109**, 245007 (2012).

[30] P. Tosi, O. Dmitrijev, Y. Soldo, D. Bassi, D. Cappelletti, F. Pirani, and V. Aquilanti, "The reaction of argon ions with hydrogen and deuterium molecules by crossed beams: Low energy resonances and role of vibronic levels of the intermediate complex," J. Chem. Phys. **99**, 985 (1993).
[31] K. M. Ervin and P. B. Armentout, "Translational energy dependence of Ar++XY→ArX++Y (XY=H2, D2, HD) from thermal to 30 eV c.m," J. Chem. Phys. **83**, 166–189 (1985).
[32] N. Laidani, R. Bartali, P. Tosi, and M. Anderle, "Argon–hydrogen rf plasma study for carbon film deposition," J. Phys. D: Appl. Phys. **37**, 2593 (2004).
[33] R. S. Mason, P. D. Miller, and I. P. Mortimer, "Anomalous loss of ionization in argon-hydrogen plasma studied by fast flow glow discharge mass spectrometry," Phys. Rev. E **55**, 7462 (1997).
[34] E. W. McDaniel and E. A. Mason, *The Mobility and Diffusion of Ions in Gases* (Wiley, New York, 1973).
[35] Yu. P. Raizer, *Gas Discharges* (Springer, Berlin, 1991).
[36] J. D. C. Jones, D. J. Lister, D. P. Wareing, and N. D. Twiddy, "The temperature dependence of the three-body reaction rate coefficient for some rare-gas atomic ion-atom reactions in the range 100-300 K," J. Phys. B: Atom. Molec. Phys. **13**, 3247 (1980).
[37] D. Magni, Ch. Deschenaux, Ch. Hollenstein, A. Creatore, and P. Fayet, "Oxygen diluted hexamethyldisiloxane plasmas investigated by means of in situ infrared absorption spectroscopy and mass spectrometry," J. Phys. D: Appl. Phys. **34**, 87 (2001).
[38] S. Carles, J. L. Le Garrec, and J. B. A. Mitchell, "Electron and ion reactions with hexamethyldisiloxane and pentamethyldisiloxane," J. Chem. Phys. **127**, 144308 (2007).
[39] A. Hallil and B. Despax, "Internal r.f. plasma parameters correlated with structure and properties of deposited hydrocarbon films," Thin Solid Films **358**, 30 (2000).